ECS Transactions, 33 (1) 991-1006 (2010)
10.1149/1.3484593 ©The Electrochemical Society

Through-mask Electro-etching for Fabrication of Metal Bipolar Plate Gas Flow Field Channels

H. McCrabb[a], E.J. Taylor[a], A. Lozano-Morales[a], S. Shimpalee[b], M. Inman[a], J. W. Van Zee[b]

[a]Faraday Technology, Inc., Clayton, OH 45315, USA
[b]Department of Chemical Engineering, University of South Carolina, Columbia, SC 29208

Transition of PEM fuel cells to the commercial market requires low-cost components, materials and manufacturing processes. Considering that bipolar plate manufacturing currently contributes to a significant percentage of the total fuel cell manufacturing cost, an inexpensive bipolar plate manufacturing process must be realized for fuel cells to achieve prominence in the commercial energy sector. A through-mask electro-etching process for high volume manufacturing of stainless steel bipolar plate gas flow field channels is being developed using pulse and pulse reverse electric fields. It has been demonstrated that the process can achieve a uniform channel depth, exhibits good repeatability for multiple experiments performed under the same conditions and the undercut beneath the photoresist mask varies linearly with channel depth indicating that pattern design compensation prior to photoresist patterning of the substrate to achieve the dimensional accuracy of the gas flow field channels and ribs is possible.

Introduction

Inexpensive components, materials and manufacturing processes are necessary for successful implementation of PEM fuel cells into the commercial marketplace. The bipolar plate is one component that contributes significantly to the total PEM fuel cell manufacturing cost (1). While graphite has been widely researched as a candidate material for the fabrication of PEM fuel cell bipolar plates due to its adequate electrical conductivity, light weight and good corrosion resistance; machining the gas flow field channels into the graphite is difficult and expensive. In addition, there are mechanical issues, such as cracking of the graphite within the stack, that have lead to the exploration of different bipolar plate materials. Metallic bipolar plates are an attractive alternative to graphite providing the necessary electrical and thermal conductivity and offering good mechanical strength to support the forces within the stack. Stainless steel, which is relatively inexpensive, sufficiently conductive, corrosion resistant and offers high strength, has shown satisfactory performance as a bipolar plate for several thousand hours of testing (2); therefore there is an interest in inexpensive manufacturing processes for stainless steel bipolar plates.

To meet the need for high volume stainless steel bipolar plate manufacturing, a through-mask electro-etching process is being developed. Through-mask electro-etching involves patterning a photoresist mask on the surface of the bare, flat stainless steel

Downloaded 23 Dec 2010 to 24.106.113.125. Redistribution subject to ECS license or copyright; see http://www.ecsdl.org/terms_use.jsp

substrate to protect specific areas during the etching process. An electric field is applied between the patterned bipolar plate substrate and a counter electrode, submerged in a benign solution, to electrochemically remove the exposed metal not protected by the photoresist mask. Once the etching process is complete, the photoresist is removed from the substrate surface to reveal the gas flow field channels. While the economic details for scale-up of through-mask electro-etching to high volume manufacturing are still being developed, preliminary analysis suggests that based upon batch manufacturing, the process should be cost-competitive and capable of meeting the DOE's 2010 target of <$5/kW for bipolar plates.

The shape of the applied electric field strongly influences the current distribution that develops on the surface of the patterned bipolar plate substrate during the through-mask electro-etching process, affecting the formation of the gas flow field channels. Pulse and pulse reverse (P/PR) electric fields are being used for the through-mask electro-etching process development in place of direct current (DC) electric fields. Pulse electric fields involve the application of an applied voltage that is periodically turned on and off for known period of times that can range from fractions of a second to seconds. In addition to turning the electric fields on and off, pulse reverse electric fields involve also periodically reversing the polarity of the substrate from anodic to cathodic during the electro-etching process. The application of P/PR electric fields instead of DC electric fields enables a higher level of process control through optimization of the pulse parameters (i.e. the frequency, pulse on-times and off-time and peak voltages).

In the present work, through-mask electro-etching for fabrication of 304L and 430 stainless steel alloy (SS304L and SS430) bipolar plates is presented. The influence of the through-mask electro-etching processing parameters on material removal rates, surface finish, accuracy and dimensional control of the gas flow field channels is discussed. SS304L and SS430 were selected for experiments because they provide an adequate compromise between strength, corrosion resistance and material cost for bipolar plate applications. SS304L and SS430 are austenitic and ferritic stainless steel alloys respectively, and while these stainless steel alloys are not as corrosion resistant as others that have been researched for bipolar plates, such as SS316, they are less expensive. It is anticipated that regardless of which stainless steel alloy is used, a conductive coating will have to be applied to the bipolar plate surface due to the protective oxide layer that forms on the stainless steel. The oxide layer provides corrosion resistance but also increases contact resistance within the fuel cell stack, and a conductive, corrosion resistant coating (e.g. flash gold) enables some of the alloy corrosion resistance to be compromised to decrease contact resistance and minimize material cost. It should also be noted that the SS430 alloy has increased mechanical strength compared with 304L and was investigated because due to the hardness of the material, SS430 is not conducive to the stamping process for formation of bipolar plate gas flow field channels.

Experimental

Substrates of SS304L, and SS430 alloy measuring 10 cm x 10 cm x 0.3 and 10 cm x 10 cm x 0.2 cm respectively were patterned with a three channel serpentine gas flow field using standard UV photolithographic techniques. The flow field measured 5.6 cm x 5.1 cm and contained channels and ribs with designed widths of 0.8 mm and 0.9 mm respectively. A photograph of the patterned bipolar plate prior to through-mask electro-

Downloaded 23 Dec 2010 to 24.106.113.125. Redistribution subject to ECS license or copyright; see http://www.ecsdl.org/terms_use.jsp

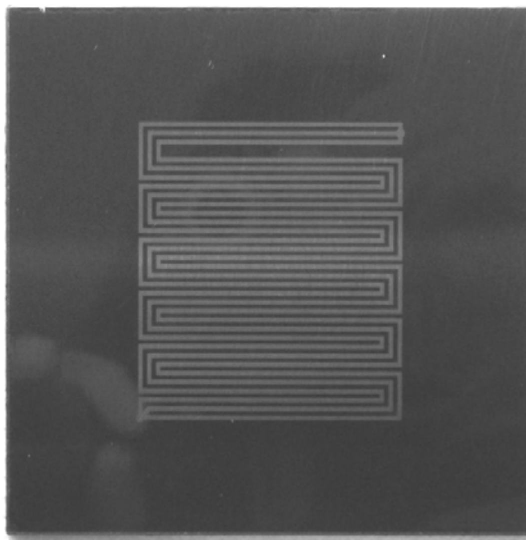

Figure 1. Photograph of A patterned stainless steel bipolar plate substrate prior to through-mask electro-etching.

etching is provided in Figure 1. The dark gray area is the photoresist and the light gray area is the exposed metal that will be electroetched into gas flow field channels. An insoluble counter electrode constructed of iridium oxide coated titanium was used for all experiments. The electrode spacing was experimentally optimized. Process parameters such as forward peak voltages, duty cycle, frequency and the addition of a reverse period by switching the polarity of the bipolar plate substrate with and without an off-time were explored in sodium nitrate (200 g/L). The forward and reverse pulsing parameters refer to an anodic bias and a cathodic bias respectively applied to the bipolar plate substrate. The period of the waveform is the summation of the forward on-time, the reverse on-time and the off-time. The forward duty cycle is the ratio of the forward on-time to the period and the reverse duty cycle is the ratio of the reverse on-time to the period. The frequency of the pulse waveform is the inverse of the period. Pulse and pulse reverse waveforms were generated with a TechNu pulse power supply, model SPR-300/100/48-3. The electrolyte solution temperature was maintained at constant ambient temperatures. Through-mask electro-etching experiments were conducted in an electrochemical cell designed to facilitate uniform flow across the surface of a flat substrate (3). A detailed description of the electrochemical cell has been provided for previous work (4).

The surface profile from the top of the bipolar plate to the bottom of the bipolar plate flow field were measured with a Mitutoyo SJ400 contact profilometer. These results provided insight on the rib width and channel depth and uniformity of the two for each test. From the rib width and channel depth, the undercut beneath the photoresist and the etch factor, i.e. the ratio of the electroetching depth to undercut beneath the photoresist, was estimated. A schematic of a cross-section of the channel illustrating the undercut is provided in Figure 2.

Downloaded 23 Dec 2010 to 24.106.113.125. Redistribution subject to ECS license or copyright; see http://www.ecsdl.org/terms_use.jsp

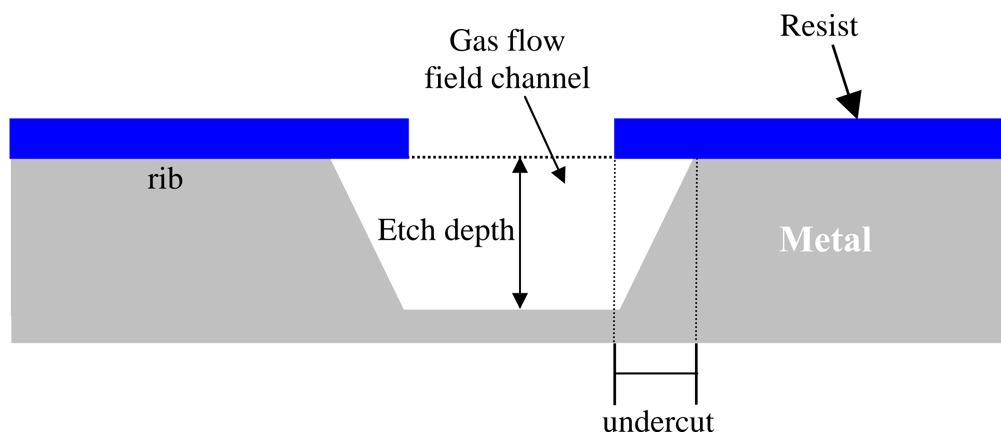

Figure 2. Schematic illustration of a gas flow field channel illustrating the undercut beneath the photoresist that occurs during through-mask electro-etching.

Results and Discussion

Effect of Pulse and Pulse Reverse Waveform Parameters on Gas Flow Field Channels

Pulse Reverse Waveform Experiments. Four pulse reverse waveform experiments were conducted to investigate the effect of temporarily switching the polarity of the bipolar plate on the formation of the gas flow field channels. The polarity of the forward pulse voltage is anodic to electroetch the gas flow field channels, and the reverse pulse voltage polarity is cathodic. The reverse pulse voltage is expected to breakdown the passive oxide layer that commonly forms on the surface of stainless steel and can slow down the electro-etching during anodic electrochemical metal removal processes. Table I provides the waveform parameters used for the experiments.

TABLE I. Pulse reverse waveform parameters for through-mask electro-etching of stainless steel bipolar plate gas flow field channels.

Experiment No.	Material	Forward Peak Voltage	Reverse Peak Voltage	Forward Duty Cycle	Reverse Duty Cycle	Frequency	Time (min)
1	SS304L	High	Low	20%	80%	Low	15
2	SS430	High	Low	5%	95%	Low	10
3	SS304L	High	Low	5%	25%	Low	82
4	SS304L	High	Low	5%	25%	Low	16

Experiments 1 and 2 used pulse reverse waveforms that did not utilize an off-time, i.e. the electric field polarity was switched periodically, but the electric field was not turned off during the experiment. Experiment 1 examined a forward duty cycle of 20%, meaning that the electric field was turned on for 20% of the experiment time. During processing, the photoresist began to delaminate from the surface of the substrate, exposing areas of the metal that were meant to be protected from the electro-etching process. This resulted in a loss of the pattern definition because both the channels and the ribs of the bipolar plate were electro-etched. It was determined that the photoresist delaminated because the lateral electro-etching rate for this experiment was too high and

Downloaded 23 Dec 2010 to 24.106.113.125. Redistribution subject to ECS license or copyright; see http://www.ecsdl.org/terms_use.jsp

an excessive amount of undercut occurred causing removal of the metal that the photoresist was adhered to. Experiment 2 used a similar waveform to Experiment 1, but the forward duty cycle was decreased to 5% in an attempt to decrease the lateral electro-etching rate and thereby minimize the undercut beneath the photoresist to prevent photoresist delamination. Subsequent to electro-etching in Experiment 2, it was noticed an undesired substance, suspected to be iron oxide film, was present within the channels and minimal electro-etching of the SS430 substrate occurred. The iron oxide film adhered strongly to the channels' surface. In this case, the time that the reverse voltage was applied was too long and likely caused deposition of the iron that was removed from the surface of the substrate during the forward portion of the waveform.

Experiments 3 and 4 used pulse reverse waveforms that incorporated an off-time. The off-time was added to the waveforms in an attempt to eliminate the iron oxide from being deposited onto surface of the channels. The forward duty cycle was the same as Experiment 2 in each case. The reverse duty cycle was reduced to 25% and the off-time applied for the remaining 70% of the time. For Experiment 3, the off-time was applied after the forward pulse and before the reverse pulse. The waveform was designed to allow electro-etching to occur during the forward pulse, followed by the off-time to enable the metal by-products, e.g. iron hydroxide and iron ions, to be flushed from the surface of the substrate and then the reverse pulse was applied to remove the thin oxide layer from the surface that develops during anodic electrochemical metal removal processes. After processing, the photoresist was removed from the substrate using an alkaline solution, to reveal the serpentine gas flow field. The addition of the off-time between the forward and reverse pulse successfully prevented the iron oxide from adhering to the channel surfaces.

A contact profilometer was used to obtain the channel profile for Experiment 3 down the centerline of the gas flow field (Figure 3). The gas flow field ribs and channels were used to calculate the average rib width and channel depth respectively. The standard deviation for the averages was calculated and the uniformity of the rib width and channel depth is reported as the coefficient of variation, CV. The CV was calculated by finding the quotient of the standard deviation of the average values divided by the average values. The channel depth, rib width and their uniformities as CV and the electro-etch rate for Experiment 3 are reported in Table II.

The channel profile in Figure 3 and results presented in Table II show that the pulse reverse waveform used in Experiment 3 (conditions listed in Table I) provided good channel depth uniformity with a calculated CV of 5% for a channel depth of 0.443 mm, however the final rib width of 0.26mm suggests that the undercut is high and the rib width uniformity is low.

Downloaded 23 Dec 2010 to 24.106.113.125. Redistribution subject to ECS license or copyright; see http://www.ecsdl.org/terms_use.jsp

Table II. Impact of using an off-time between the forward and reverse pulse on gas flow field ribs and channels.

Experiment No.	Avg. Channel Depth (mm)	Avg. Channel Depth CV (%)	Avg. Rib Width (mm)	Avg. Rib Width CV (%)	Etch rate (μm/min)
3	0.443	5.3	0.26	18	5.4

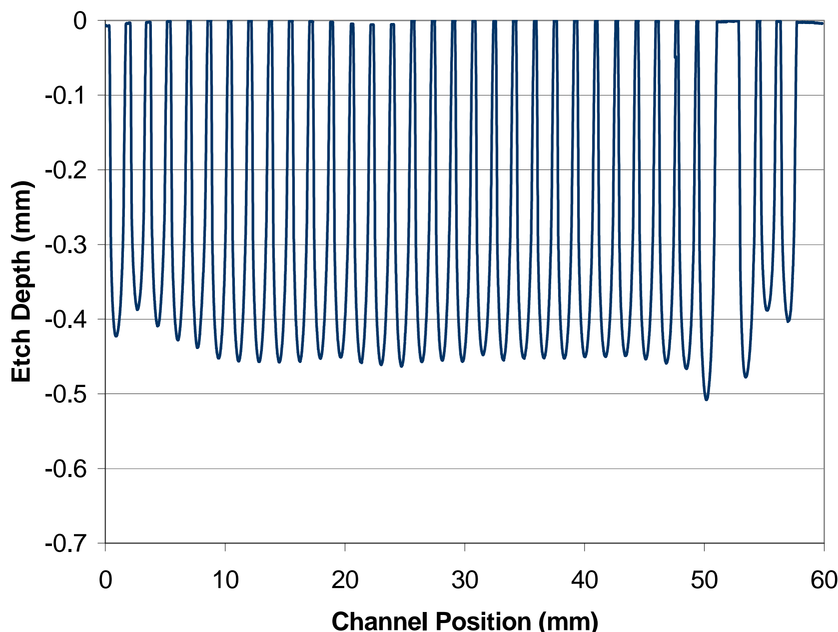

Figure 3. Channel profile plot showing the channel depth and rib width for the gas flow field etched in Experiment 3.

The undercut beneath the photoresist can be determined by taking the difference of the initial photoresist width (0.9 mm) and the average rib width and dividing by 2. Because each experiment yielded a different average channel depth, the etch factor, which is the ratio of the channel depth to the undercut is used to compare the vertical electro-etching to the lateral electro-etching for each experiment. To minimize the undercut beneath the photoresist, it is desirable to obtain a high etch factor, which indicates the vertical electro-etching rate is higher than the lateral electro-etching rate. The undercut and etch factor for Experiment 3 were calculated to be 0.32 mm and 1.4 respectively.

Experiment 4 was performed using the same conditions as Experiment 3 except the waveform consisted of the forward pulse, followed by the reverse pulse and finally the off-time was applied. Changing the placement of the off-time significantly affected the formation of the gas flow field channels when compared with the results in Experiment 3. Minimal metal removal occurred during processing due to a significant amount of iron hydroxide precipitate blocking the surface of the channels. Without the off-time immediately following the forward pulse to flush away the iron hydroxide produced during the forward pulse, the reverse pulse deposited the iron hydroxide precipitate that was produced near the substrate surface during the forward pulse instead of removing the

Downloaded 23 Dec 2010 to 24.106.113.125. Redistribution subject to ECS license or copyright; see http://www.ecsdl.org/terms_use.jsp

thin passive oxide layer from the stainless steel surface. The result was minimal electro-etching, however a mirror-like surface finish of the channels was achieved.

Pulse Waveform Experiments. In an effort to reduce the channel electro-etching rate and decrease the undercut, the reverse pulse was removed so that only a forward anodic pulse and an off-time were used to electro-etch the gas flow fields. The forward pulse will electro-etch the gas flow field channels into the metal surface, and the off-time will allow for the iron hydroxide precipitate formed as a by-product during the forward pulse to be removed from the channel surface by forced convection and diffusion. Table III contains the pulse waveform parameters used for Experiments 5 and 6.

TABLE III. Pulse waveform parameters for through-mask electro-etching of stainless steel bipolar plate gas flow field channels.

Experiment No.	Material	Forward Peak Voltage	Forward Duty Cycle	Frequency	Time(min)
5	SS430	High	20%	Low	30
6	SS430	High	5%	Low	120

Experiments 5 and 6 were operated at the same conditions except that the duty cycle of the waveform for Experiment 5 was 20% and the duty cycle of Experiment 6 was decreased to 5%. The channel profiles for these two experiments are provided in Figure 4 and the channel depths, rib widths and their uniformities as CV and the electro-etching rates are reported in Table IV.

Table IV. Impact of pulse parameters with varying duty cycles on gas flow field ribs and channels.

Experiment No.	Avg. Channel Depth (mm)	Avg. Channel Depth CV (%)	Avg. Rib Width (mm)	Avg. Rib Width CV (%)	Etch rate (μm/min)
5	0.247	10	0.26	9.1	8.3
6	0.363	7.3	0.42	5.1	3.1

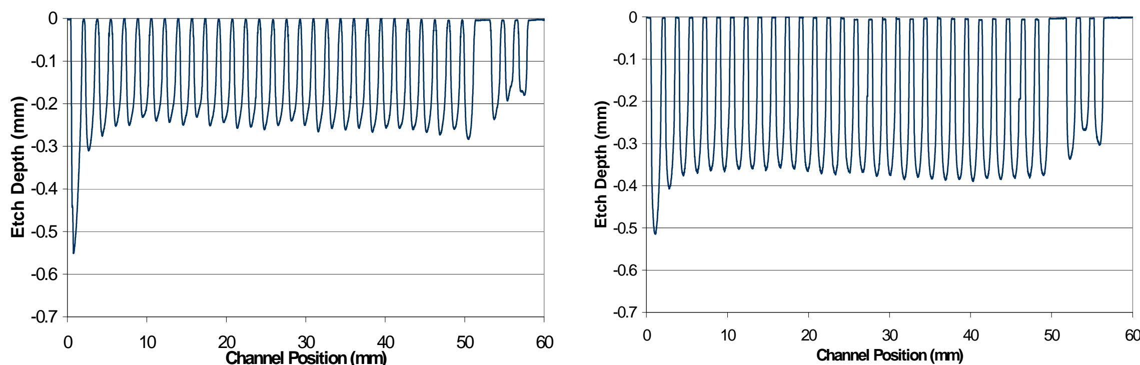

Figure 4. Channel profile plot showing the channel depth and rib width for the gas flow field etched in Experiments 5 (left) and 6 (right).

For a duty cycle of 20%, the exclusion of the reverse pulse led to an improved rib width uniformity compared with Experiment 3, however the uniformity of the channel

Downloaded 23 Dec 2010 to 24.106.113.125. Redistribution subject to ECS license or copyright; see http://www.ecsdl.org/terms_use.jsp

depth was compromised. Additionally, the undercut for Experiment 6 was the same as Experiment 3 at 0.32 mm, however the channel depth for Experiment 6 was more shallow, leading to an undesirable decrease in the etch factor to 0.8.

By decreasing the duty cycle from 20 to 5 %, the undercut was reduced from 0.32 mm to .24 mm (a 25 % reduction) resulting in an average rib width of 0.42 mm for Experiment 6. In addition, because the channel depth for Experiment 6 was greater than that of Experiment 5, the etch factor increased from 0.8 to 1.5. The improvement in the vertical electro-etching rate is attributed to slowing down the electro-etching rate to provide a more controlled electro-etching process. The uniformity of the channel depth for Experiment 6 is greater than that of Experiment 5, though slightly lower than that of Experiment 3. The rib width uniformity is quite good at ~ 5% for Experiment 6.

Cell Geometry to Control Uniformity of Channel Depth and Rib Width for Gas Flow Fields

When electro-etching a substrate that is partially covered with an insulating material (e.g. a photoresist mask), it is well known that edge effects can cause the current density distribution to be nonuniform, even when the electrode is recessed slightly, due to the finite thickness of the insulating material. A common, practical and economic scenario is one in which a counter electrode is placed parallel to the working electrode at a relatively small distance, and the counter electrode is masked to improve uniformity. Faraday has previously studied the variation of counter electrode size to control current distribution in parallel plate cells (5), and this knowledge was used to improve the channel depth and rib width uniformity.

The pulse waveform from Experiment 6 (Table III) was used for these experiments and the bipolar plate substrate was SS430. The anode to cathode ratio was held constant at 1.25. For Experiment 7, the cathode (i.e. the counter electrode) was shifted 5 mm upwards from its original location in the electro-etching cell. The location of the cathode was determined by examining the channel profile obtained in Experiment 6 (Figure 5, top) and realizing that the channels ~ 5 mm from the bottom of the bipolar plate were etched too deep and the channels ~ 5 mm from the top of the bipolar plate were etched too shallow. Therefore shifting the cathode location upward for Experiment 7 should focus more of the current toward the top of the plate, while reducing the current focused at the bottom of the plate. Figure 5 shows the channel profile plots with schematic illustrations of the positioning of the cathode relative to the gas flow field pattern within the electrochemical cell for Experiments 6 and 7, and Table V provides the channel depths, rib widths and their uniformities as CV for these experiments.

Table V. Impact of the placement of the cathode relative to the bipolar plate gas flow field pattern within the electrochemical cell during through-mask electro-etching.

Experiment No.	Avg. Channel Depth (mm)	Avg. Channel Depth CV (%)	Avg. Rib Width (mm)	Avg. Rib Width CV (%)
6	0.363	7.3	0.42	5.1
7	0.421	16	0.38	21.1
8	0.403	8.7	0.40	6.9

Downloaded 23 Dec 2010 to 24.106.113.125. Redistribution subject to ECS license or copyright; see http://www.ecsdl.org/terms_use.jsp

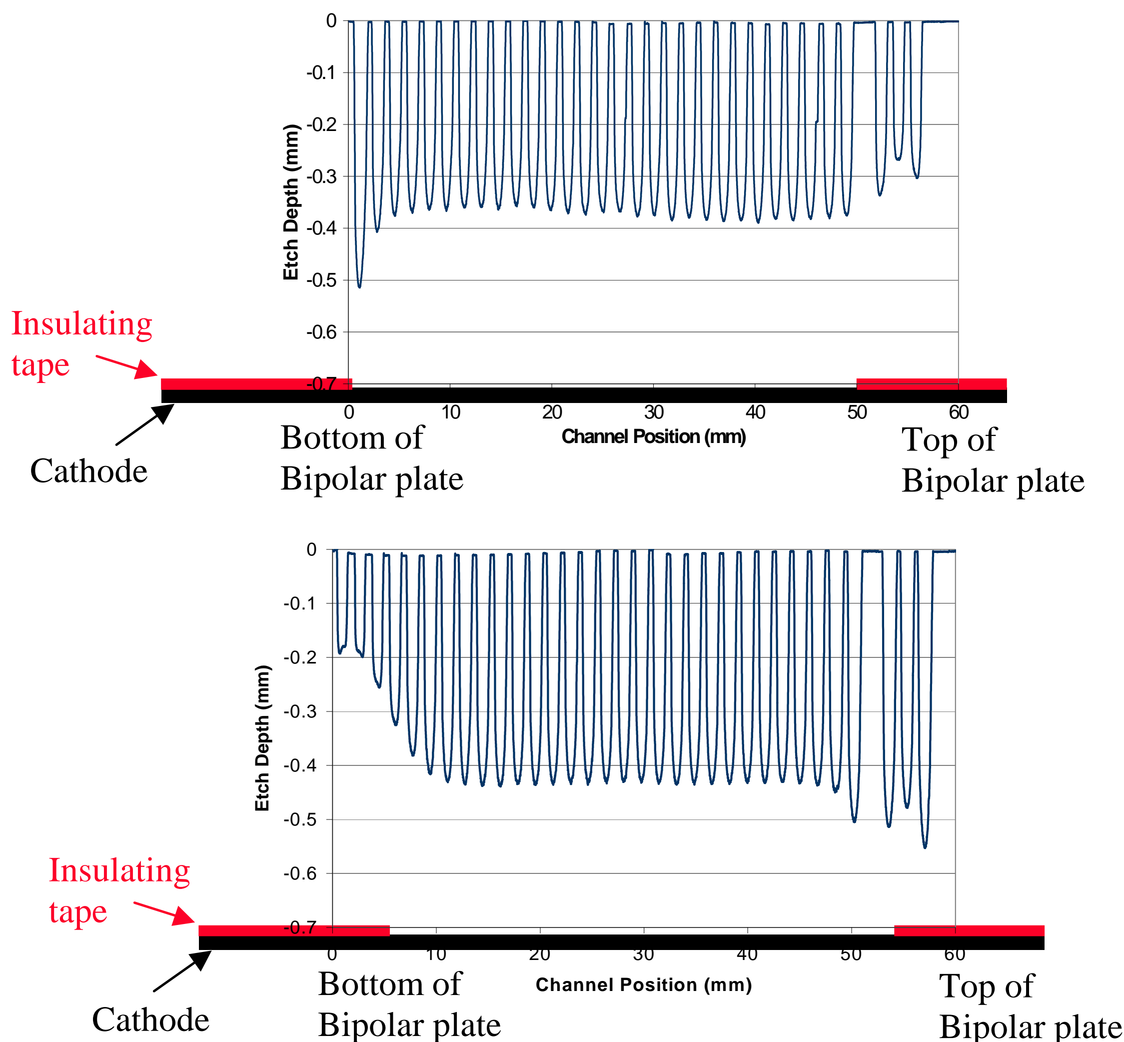

Figure 5. Channel profile plots for Experiments 6 (top) and 7 (bottom) indicating the positioning of the cathode relative to the gas flow field pattern within the electrochemical cell used for the through-mask electro-etching experiments.

By repositioning the cathode as described above, the channel depth profile changed noticeably. The channels at the bottom of the bipolar plate became shallower than the channels above and the channel depth at the top of the plate increased beyond the channels below. The overall uniformity of the channel depth and rib widths for Experiment 7 decreased when compared with Experiment 6. The undercut for Experiment 7 was 0.26 mm and the etch factor of 1.6 was comparable to Experiment 6.

The cathode was again repositioned within the electrochemical cell for Experiment 8. It was shifted 3 mm down from where it was located in Experiment 7. The channel profile plot illustrating the positioning of the cathode relative to the gas flow field pattern within the electrochemical cell is provided in Figure 6.

Downloaded 23 Dec 2010 to 24.106.113.125. Redistribution subject to ECS license or copyright; see http://www.ecsdl.org/terms_use.jsp

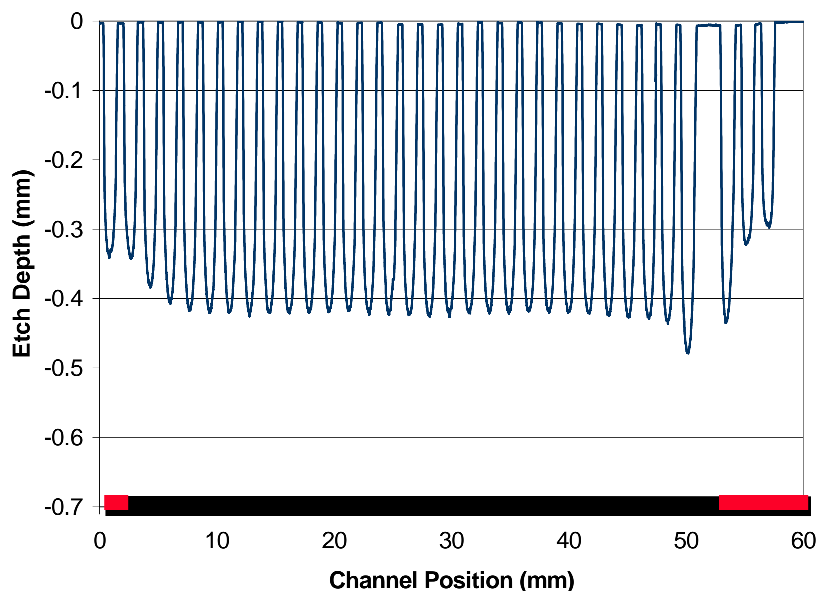

Figure 6. Channel profile plots for Experiments 8 indicating the positioning of the cathode relative to the gas flow field pattern within the electrochemical cell used for the through-mask electro-etching experiments.

The overall channel depth and rib width uniformity for Experiment 8 was better than Experiment 7 and similar to Experiment 6 (See Table V). The undercut for Experiment 8 was 0.25 mm and the etch factor was the same as Experiment 7 at 1.6

Effect of Experiment Time on Electro-etching Rate Channel Depth, Undercut and Etch Factor

Effect of Experiment Time on Electro-etching SS430. The pulse waveform applied in Experiment 8 was applied for three additional experiments at various processing times to examine the effect of processing time on electro-etching rate, the channel depth, undercut and the etch factor using SS430 as the bipolar plate substrate. Figure 7 provides the channel profile plots Experiments 8 - 11 obtained at four different electro-etching times: 40 minutes (A), 82 minutes (B), 100 minutes (C) and 130 minutes (D). and Table VI provides the channel depths, rib widths and their uniformities as CV and the electro-etching rates.

Table VI. Impact of varying the electro-etching time during through-mask electro-etching for Experiments 8 – 11.

Experiment No.	Time (min)	Avg. Channel Depth (mm)	Avg. Channel Depth CV (%)	Avg. Rib Width (mm)	Avg. Rib Width CV (%)	Etch rate (µm/min)
8	82	0.403	8.7	0.40	6.9	4.9
9	100	0.428	8.4	0.37	10.2	4.3
10	130	0.529	7.4	0.24	13.8	4.1
11	40	0.208	8.7	0.63	4.6	5.2

Downloaded 23 Dec 2010 to 24.106.113.125. Redistribution subject to ECS license or copyright; see http://www.ecsdl.org/terms_use.jsp

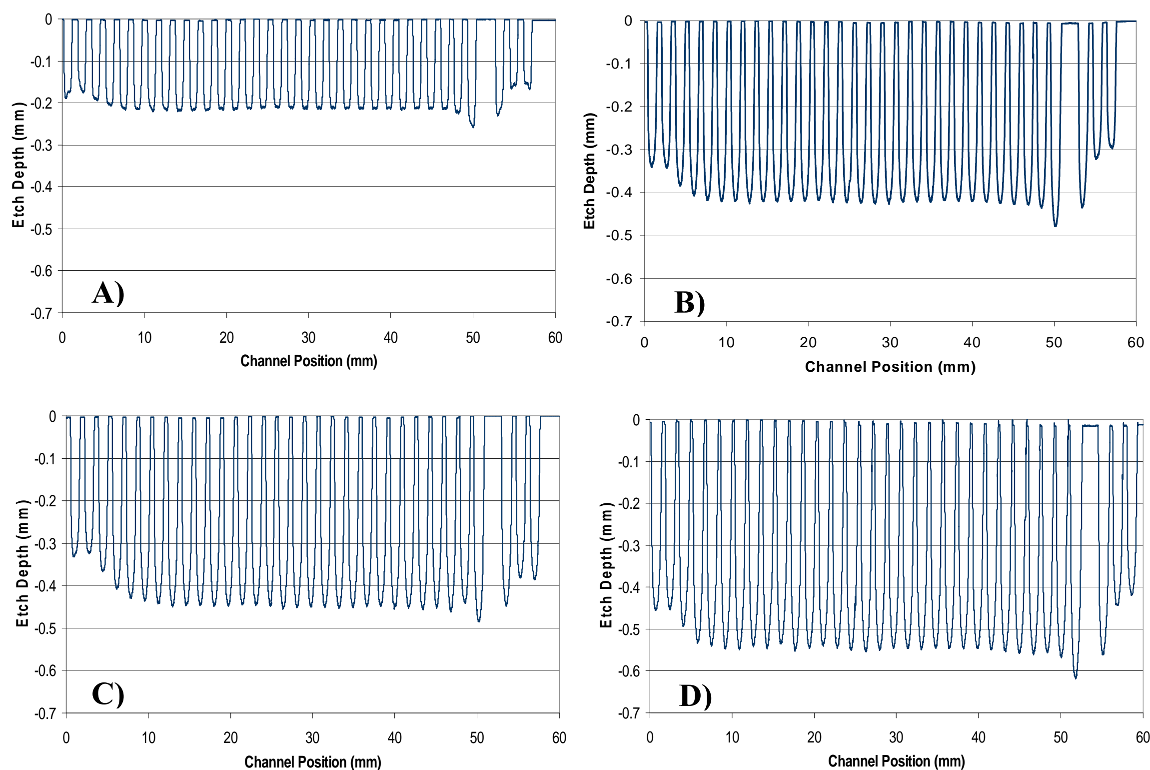

Figure 7. Channel profile plots for Experiments 8 – 11 at various electro-etching times. A) Experiment 11 at 40 min., B) Experiment 8 at 82 min., C) Experiment 9 at 100 min. and D) Experiment 10 at 130 min.

All channel depth profiles are nearly uniform across the SS430 bipolar plate and nearly flat. Further adjustments could be made to the cathode placement within the electrochemical cell if the fuel cell stack performance indicates a completely flat profile is required. It should be noted that the rib width uniformity seems to decrease with increasing electro-etching time, i.e. as the channel depth increases.

Figure 8 shows a plot of the average channel depth and etch rate versus etching time after electro-etching Experiment 8 – 11. The target channel depth is 550 µm, which was almost achieved after 130 min (average channel depth equals to 529 µm). The plot in Figure 8 shows that the channel depth varies linearly with time and the electro-etching rate decreases with time. The electro-etching rate was 5.2 µm/min at an average channel depth of 208 µm, decreasing slightly to 4.9 µm/min at an average channel depth of 403 µm. The etch rate decreased considerably from 4.9 µm/min to 4.3 µm/min at an average channel depth of 428 um, decreasing slightly to 4.1 µm/min at an average channel depth of 529 µm.

Figure 9 shows the average channel depth and etch factor versus undercut after electro-etching in Experiments 8 – 11. The average channel depth versus undercut data are linear with a correlation greater than 0.99. Moreover, the slope of the linear regression equals 1.6, which is consistent with the almost constant value of ~1.6 observed for the etch factor.

Downloaded 23 Dec 2010 to 24.106.113.125. Redistribution subject to ECS license or copyright; see http://www.ecsdl.org/terms_use.jsp

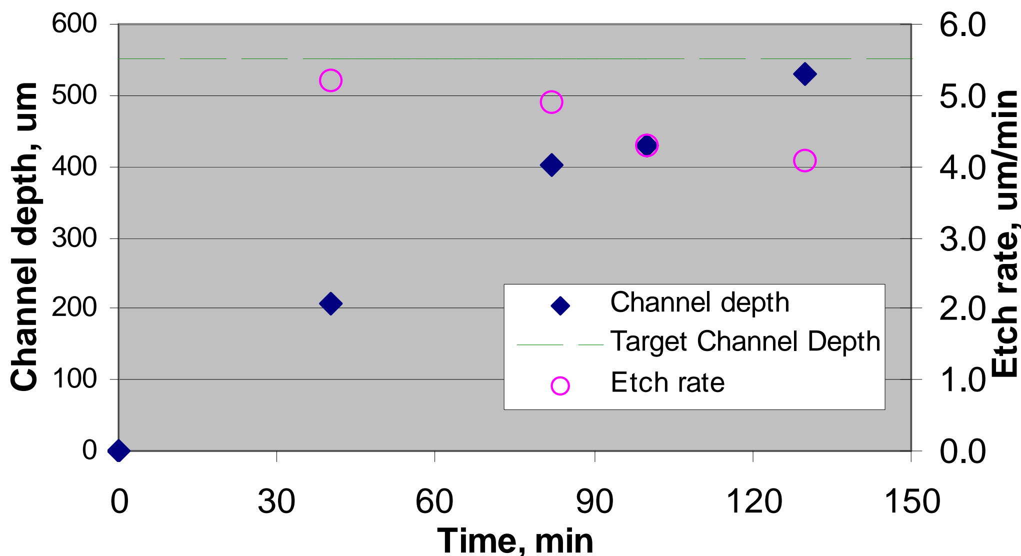

Figure 8. Average channel depth and etch rate vs. etching time for Experiments 8 – 11.

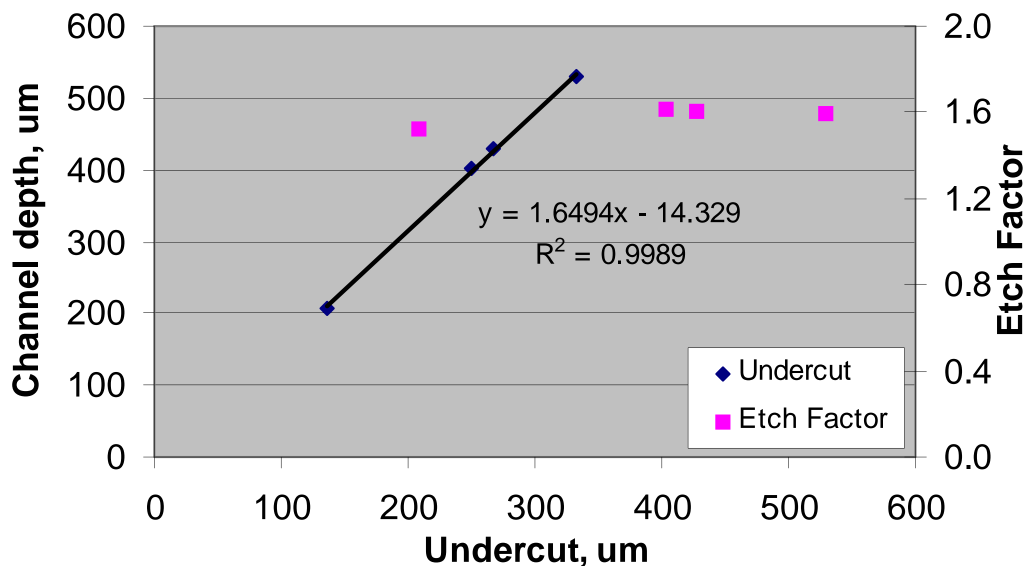

Figure 9. Average channel depth and etch factor vs. undercut for Experiments 8 – 11.

Effect of Experiment Time on Electro-etching SS304L. The pulse waveform applied in Experiment 8 was applied for three additional experiments at various processing times to examine the effect of processing time on electro-etching rate, the channel depth, undercut and the etch factor using SS304L as the bipolar plate substrate. Figure 10 provides the channel profile plots Experiments 12 - 15 obtained at four different electro-etching times: 40 minutes (A), 82 minutes (B), 100 minutes (C) and 130 minutes (D)., and Table VII provides the channel depths, rib widths and their uniformities as CV and the electro-etching rates.

Downloaded 23 Dec 2010 to 24.106.113.125. Redistribution subject to ECS license or copyright; see http://www.ecsdl.org/terms_use.jsp

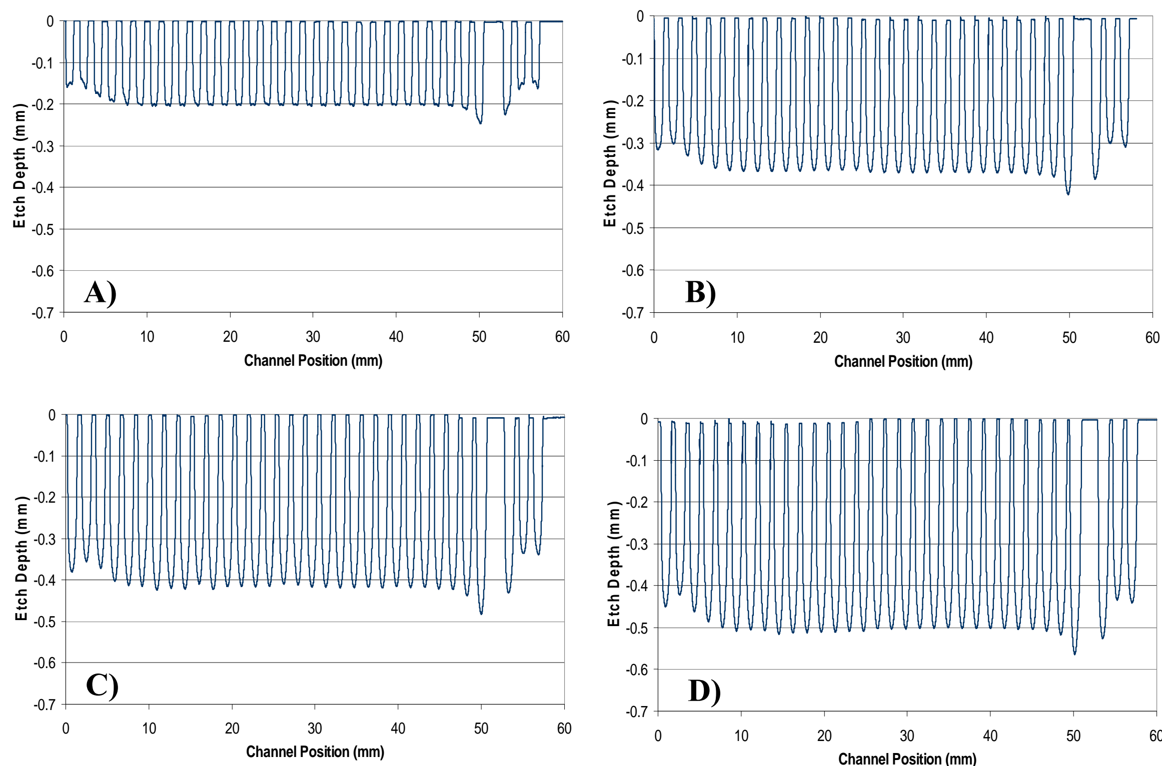

Figure 10. Channel profile plots for Experiments 12 – 15 at various electro-etching times. A) Experiment 12 at 40 min., B) Experiment 13 at 82 min., C) Experiment 14 at 100 min. and D) Experiment 15 at 130 min.

Table VII. Impact of varying the electro-etching time during through-mask electro-etching for Experiments 12 – 15.

Experiment No.	Time (min)	Avg. Channel Depth (mm)	Avg. Channel Depth CV (%)	Avg. Rib Width (mm)	Avg. Rib Width CV (%)	Etch rate (µm/min)
12	40	0.196	9.2	0.65	2.9	4.9
13	82	0.357	6.7	.45	5.1	4.4
14	100	0.405	6.7	0.39	5.6	4.1
15	130	0.497	6.2	0.28	10.6	3.8

Similarly to the SS430 electro-etched in Experiments 8 – 11, all of the channel profiles shown in Figure 10 are nearly uniform across the SS304L plate in Experiments 12 – 15. Figure 11 shows a plot of the average channel depth versus etching time after electro-etching SS304L and SS430 bipolar plates in Experiments 12 – 15 and 8 – 11 respectively. The electro-etching rate decreases for both materials. In addition, the electro-etching rate (and therefore etch depth at same time) is greater for SS430 compared with SS304L.

Downloaded 23 Dec 2010 to 24.106.113.125. Redistribution subject to ECS license or copyright; see http://www.ecsdl.org/terms_use.jsp

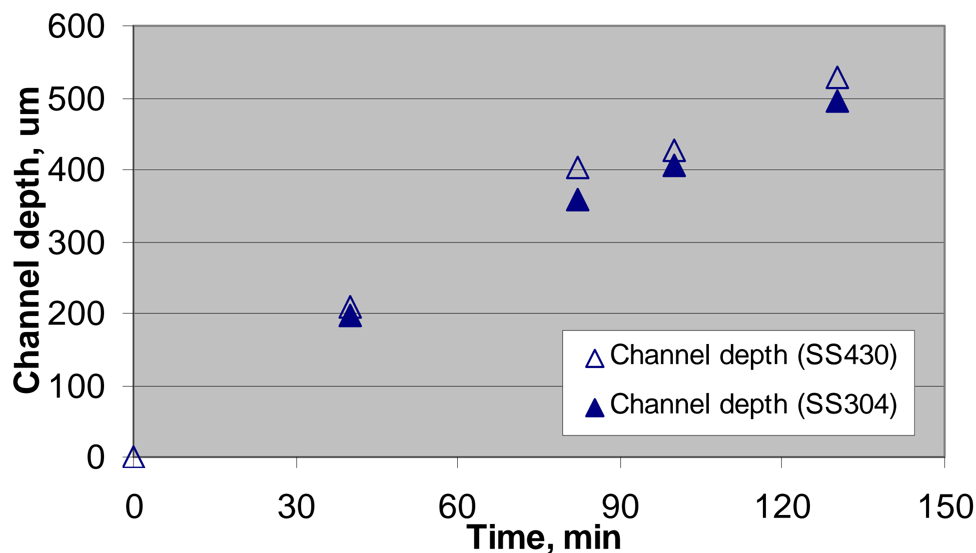

Figure 11. Average channel depth versus etching time after electro-etching SS 304L and 430 plates in Experiments 12 – 15 and 8 – 11 respectively.

Figure 12 shows the etch factor versus average channel depth after electro-etching SS304L and SS430 bipolar plates in Experiments 12 – 15 and 8 – 11 respectively. The etch factor is about the same for both materials (i.e. 1.6). Similar to SS430, the average channel depth versus undercut data are linear with a correlation greater than 0.99. Moreover, the slope of the linear regression equals 1.6, which is consistent with the almost constant value of ~1.6 observed for the etch factor. Because the undercut beneath the photoresist mask varies linearly with channel depth for both materials, pattern design compensation prior to application of the photoresist to achieve the dimensional accuracy of the gas flow field channels and ribs is possible.

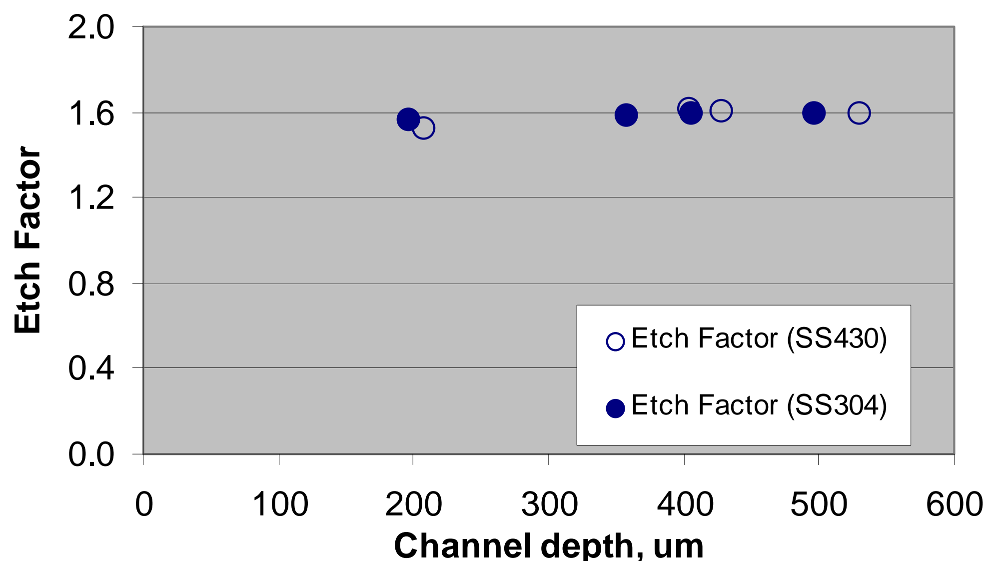

Figure 12. Etch factor versus channel depth after electro-etching SS304L and SS430 bipolar plates in Experiments 12 – 15 and 8 – 11 respectively.

Downloaded 23 Dec 2010 to 24.106.113.125. Redistribution subject to ECS license or copyright; see http://www.ecsdl.org/terms_use.jsp

Process Repeatability

Experiments 16 and 17 were performed under the exact same conditions as Experiment 13 to examine the process repeatability. Table VIII provides the channel depths, rib widths and their uniformities as CV and the electro-etching rates for these three tests. The results in Table VIII indicate that process repeatability is good, even after several experiments have been conducted in the same electrolyte. Figure 13 provides a plot of the channel depth vs. cumulative Amp·hours per liter for the 200 g/L $NaNO_3$ electrolyte. The results in Table VIII and Figure 13 indicates that the electrolyte maintenance is minimal for the through-mask electro-etching, making it suitable for a high volume manufacturing process for stainless steel bipolar plates.

Table VIII. Analysis of process repeatability for electro-etching SS304L for 82 minutes using a pulse waveform with a 5% duty cycle.

Experiment No.	Time (min)	Avg. Channel Depth (mm)	Avg. Channel Depth CV (%)	Avg. Rib Width (mm)	Avg. Rib Width CV (%)	Etch rate (µm/min)
13	82	0.357	6.7	.45	5.1	4.4
16	82	0.346	6.4	0.46	4.8	4.2
17	82	0.359	6.1	0.46	4.1	4.4

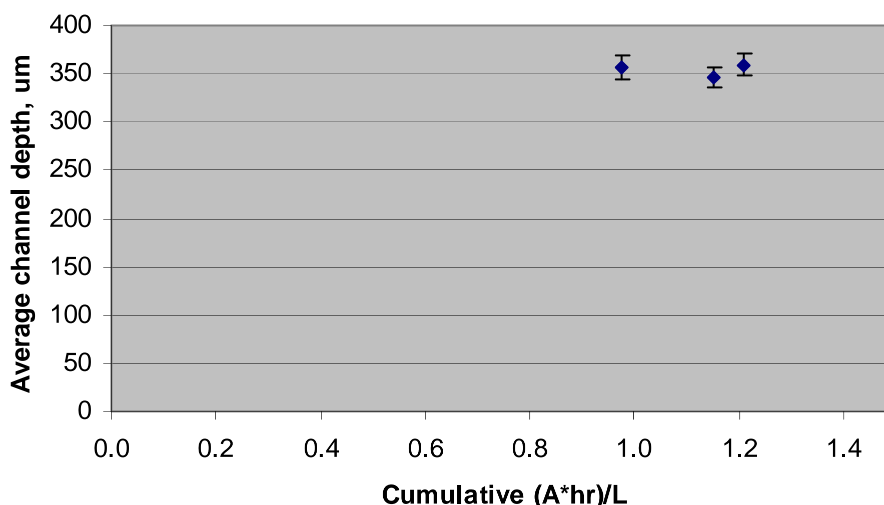

Figure 13. Plot of average channel depth vs. cumulative Amp·hours per liter for the 200 g/L $NaNO_3$ for Experiments 13, 15 and 16.

Conclusion

For PEM fuel cells to be successfully implemented into the commercial marketplace, an inexpensive, high volume bipolar plate manufacturing process will need to be developed. This work described a through-mask electro-etching process for fabrication of gas flow field channels on stainless steel bipolar plates. Results of experiments showed that a pulsed electric field and optimal placement of the electrodes within the

Downloaded 23 Dec 2010 to 24.106.113.125. Redistribution subject to ECS license or copyright; see http://www.ecsdl.org/terms_use.jsp

electrochemical cell could provide good channel depth and rib width uniformity for both SS430 and SS304L bipolar plates. The etch factor, which is the ratio of the vertical electroetching depth to the undercut beneath the photoresist, remains constant for all channel depths investigated indicating that pattern design compensation prior to photoresist patterning of the substrate to achieve the dimensional accuracy of the gas flow field channels and ribs is possible. Process repeatability was demonstrated at various Amp·hours per liter for the 200g/L $NaNO_3$ electrolyte suggesting that electrolyte maintenance would be low if the through-mask electroetching process is implemented into a manufacturing environment.

Acknowledgments

This material is based upon work supported by the DOE under Grant No. DE-FG02-08ER85112 and the NSF-Industry/University Cooperative Research Center for Fuel Cells (Grant # IIP 0856055). Any opinions, findings, and conclusions or recommendations expressed in this material are those of the authors and do not necessarily reflect the views of the DOE or NSF.

References

1. B. Cunningham and D. Baird, *J. Mater. Chem.*, **16**, 4385 (2006).
2. D. P. Davis, P.L. Adcock, M. Turpin and S.J. Rowen, J. of Power Sources, 86, 237-242 (2000).
3. L. Gebhart, J. Sun, P. Miller, E.J. Taylor "Electroplating cell with hydrodynamics facilitating more uniform deposition across a workpiece during plating", U.S. Patent No. 7,553,401 issued June 30, 2010.
4. H. McCrabb, A. Lozano-Morales, S. Snyder, L. Gebhart, E.J. Taylor, "Through Mask Electrochemical Machining" ", ECS Trans. **19** (26), 19 (2009).
5. A. Lozano-Morales, H. McCrabb, E. J. Taylor, A. C. West, "Variation of counterelectrode size to control current distribution in parallel plate cells", Manuscript submitted, J. Appl. Surf. Finish., (2007).

Downloaded 23 Dec 2010 to 24.106.113.125. Redistribution subject to ECS license or copyright; see http://www.ecsdl.org/terms_use.jsp